International Journal of Hydrological and Environmental for Sustainability
Volume 4, Issue 3, 135-148.
e_ISSN: 2828-5050
https://www.journal.foundae.com/index.php/ijhes

Analysis of Subsurface Faults Using 3D Gravity Method Based On Satellite Image Data: Insights into Indo-Australian and Eurasian Plate Subduction in the Formation of An Accretionary Prism

Kadek Ciptani Satria Dewi
Department of Physics,
Institut Teknologi Sumatera,
INDONESIA

Rahmat Nawi Siregar*
Department of Physics,
Institut Teknologi Sumatera,
INDONESIA

Trisna Ikhsan Ningati
Department of Physics,
Institut Teknologi Sumatera,
INDONESIA

Zumaida Nur Pulungan
Departement of Biosystems Engineering,
Institut Teknologi Sumatera,
INDONESIA

Agapetalia Indriyawati
Departement of Biosystems Engineering,
Institut Teknologi Sumatera,
INDONESIA

Hirotaka Takahashi
Department of Design and Data Science,
Tokyo City University,
JAPAN

***Correspondence: E-mail:** rahmat.siregar@fi.itera.ac.id

Article Info

Article history:

Received: August 10, 2025
Revised: October 15, 2025
Accepted: October 30, 2025

Abstract

This geophysical study employs the gravity method to analyze subsurface fault structures in the Simeulue Island region. The area lies within an active tectonic zone where the Indo-Australian Plate subducts beneath the Eurasian Plate, making it a critical site for understanding subduction dynamics and accretionary prism formation. Secondary gravity and topographic data were acquired from TOPEX satellite imagery. The primary objective is to identify gravity anomalies and delineate subsurface geological features such as faults, folds, and fractures based on variations in the Earth's gravitational field caused by density contrasts between rock units. The gravity method is particularly effective due to its sensitivity to such density differences. Qualitative interpretation was conducted using Surfer 16, while quantitative modeling utilized Oasis Montaj. Results reveal high Bouguer anomaly values in the southwest, corresponding to the plate convergence zone, and low anomaly values extending from the southeast to northwest, associated with the accretionary prism. The 2D model illustrates the subduction of oceanic crust with a density of 3.43 g/cm^3 beneath continental crust with a density of 2.67 g/cm^3. The 3D model further reveals that subduction becomes evident at a depth of approximately 16.11 km, with the crustal thickness in the accretionary prism zone reaching around 19.92 km. The 3D approach provides a more comprehensive spatial visualization of the subduction geometry and density distribution, offering insights that surpass conventional 2D analysis. These findings contribute to a deeper understanding of regional geodynamics and may serve as a reference for seismotectonic studies and disaster mitigation efforts in the surrounding area.

Keywords: gravity method; subsurface fault analysis; 3d modeling; plate subduction; accretionary prism; satellite gravity data

To cite this article: Dewi, K, C, S., Siregar, R, N., Ningati, T, I., Pulungan, Z, N., Indriyawati, A. and Takahashi, H. (2025). Analysis of Subsurface Faults Using 3D Gravity Method Based On Satellite Image Data: Insights into Indo-Australian and Eurasian Plate Subduction in the Formation of An Accretionary Prism. *International Journal of Hydrological and Environmental for Sustainability, 4*(3), 135-148. https://doi.org/10.58524/ijhes.v4i3.960

INTRODUCTION

The study of subsurface geological structures plays a pivotal role in understanding tectonic processes, particularly in regions characterized by active plate convergence. One such region is the western margin of Sumatra, where the Indo-Australian Plate subducts beneath the Eurasian Plate,

forming a complex accretionary prism system. This tectonic interaction has significant implications for seismic activity, crustal deformation, and the evolution of geological features such as faults, folds, and fractures (Hariyono & S, 2018; Utama et al., 2021).

Pulau Simeulue, located off the western coast of Sumatra, lies within this dynamic tectonic zone and serves as a strategic site for investigating subduction-related phenomena (Stern, 2018; Tabei et al., 2002; Yan et al., 2024). The island has experienced multiple large-magnitude earthquakes and tsunamis, underscoring the importance of detailed geophysical analysis to assess subsurface conditions and potential hazards. Despite its geological significance, comprehensive subsurface mapping in this area remains limited (H. Li et al., 2014; Yan et al., 2024).

Gravity methods offer a powerful tool for delineating subsurface structures due to their sensitivity to density contrasts between rock units. Variations in gravitational anomalies can reveal hidden fault zones, crustal discontinuities, and the geometry of subducting slabs. When integrated with satellite-derived topographic data, gravity analysis becomes even more effective in capturing regional-scale features with high spatial resolution (Ismullah et al., 2018; Watlet et al., 2020).

Recent advances in 3D gravity modeling have enabled researchers to move beyond traditional 2D interpretations, allowing for more accurate visualization of subsurface geometries. These models can simulate the depth, orientation, and density distribution of geological bodies, providing insights into the mechanics of plate interaction and the architecture of accretionary prisms. Such approaches are particularly valuable in complex tectonic settings like Simeulue island (Nishimura et al., 1986; Triani et al., 2021).

Understanding the role of fault systems in controlling geothermal fluid migration and heat distribution is essential for delineating productive zones and recharge areas. Faults can act either as conduits or barriers, depending on their orientation, permeability, and lithological context. Therefore, identifying and characterizing these structures is a key step in reducing exploration risk and improving resource assessment (Zheng et al., 2021).

In this study, gravity and topographic data obtained from TOPEX satellite imagery are utilized to construct both 2D and 3D models of the subsurface beneath Pulau Simeulue. Qualitative interpretation is performed using Surfer 16, while quantitative modeling is conducted with Oasis Montaj software. The integration of these tools facilitates a multi-scale analysis of gravitational anomalies and their geological implications (Iqbal et al., 2023). By integrating geophysical data with geological context, the research seeks to contribute to a more accurate structural interpretation of the accretionary prism in the subduction zones.

Regional Geology and Topography of Simeulue Island

Simeulue Island is located off the northwest coast of Sumatra and lies within an active subduction zone between the Indo-Australian and Eurasian Plates. This region forms part of the Sunda megathrust, which extends from western Sumatra to southern Java and is recognized as one of the most seismically active zones in the world. Tectonic activity in this area has produced a complex array of geological structures, including strike-slip faults, folds, and subduction-related features that contribute to the formation of an accretionary prism along the Sumatra Trench (Rizki et al., 2022).

Stratigraphically, the Simeulue region is dominated by sedimentary rocks ranging from the Tertiary to Quaternary periods, which have undergone deformation due to compressional forces from plate convergence. These rock units are arranged in anticlines and synclines that trend parallel to the direction of subduction (Iqbal et al., 2023). In the southwestern part of the island, a contact zone between oceanic and continental crust is marked by increased rock density and heightened seismic activity (Gan et al., 2017; C. F. Li, 2011).

The accretionary prism, which stretches from the southeast to the northwest of Simeulue, is formed by the accumulation and deformation of sediments scraped off the subducting oceanic plate. This prism exhibits distinct geophysical characteristics, such as low gravity anomalies and variable crustal thickness. Its internal structure consists of folded and faulted sedimentary layers, along with active fault zones that reflect ongoing tectonic deformation (He, 2014; Tabei et al., 2002; Taira, 2001).

Topographically, Simeulue Island exhibits a rugged terrain with elevations ranging from sea level to over 300 meters above mean sea level **(Figure 1)**. The island's topography is influenced by both tectonic uplift and erosional processes. Coastal terraces, uplifted coral reefs, and steep escarpments are common features, particularly along the western and southern coasts, indicating

recent and ongoing tectonic activity. Inland areas are dominated by rolling hills and dissected plateaus, while river valleys and alluvial plains are found in the lower-lying eastern regions. Previous studies have documented several major earthquakes in the region, including the devastating events of 2004 and 2005 that triggered widespread tsunamis. These occurrences highlight the urgent need for detailed subsurface mapping to better understand deformation mechanisms and assess future geological hazards. In this context, geophysical methods such as gravity surveys are highly effective for revealing the geometry and dynamics of subduction zones (Bronto et al., 2012; Nishimura et al., 1986).

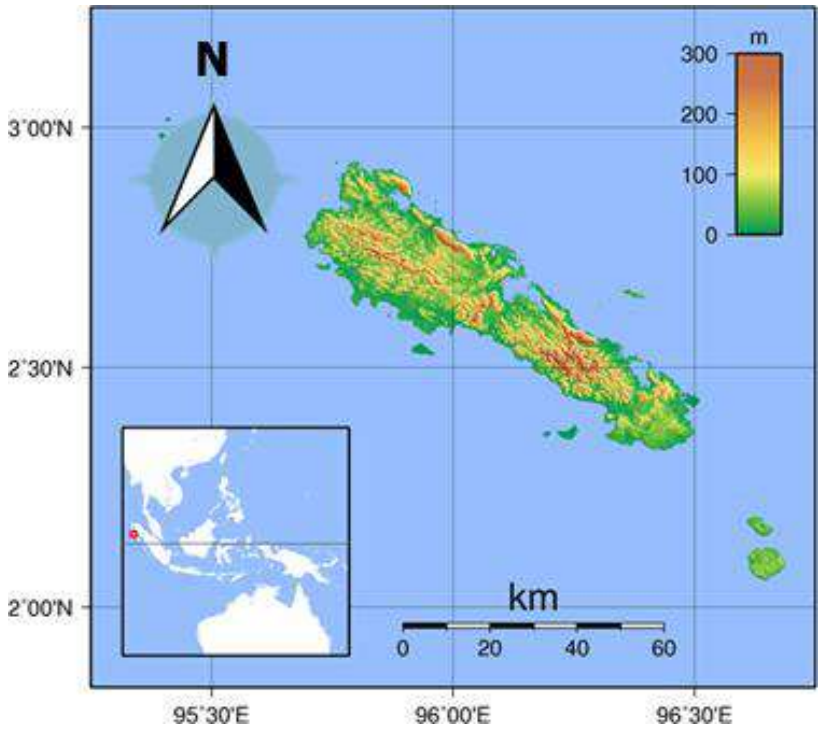

Figure 1. Map of topographically Simeulue island, North Sumatra, Indonesia

The regional geological characteristics provide a crucial framework for interpreting gravity data. Density contrasts between sedimentary layers, basement rocks, and oceanic crust generate variations in the gravitational field that can be used to identify key geological structures. By integrating satellite imagery and 3D modeling, gravity analysis enables more precise delineation of subsurface features and tectonic interactions (Lei et al., 2019; Yu-feng et al., 2021; Zhang et al., 2021). Overall, the geology of Simeulue Island reflects the complexity of an active subduction system that shapes the accretionary prism and influences crustal dynamics along the western margin of Sumatra. Understanding these geological conditions is essential for interpreting gravity modeling results and for drawing broader tectonic implications (Siregar et al., 2022).

METHOD

Data Acquisition and Processing Timeline

This research was conducted on Simeulue Island, located at 1º59' S - 3º14' S and 95º6' E - 96º59' E. The research was conducted from November 2021 to May 2022, with data processing carried out at the Earth Physics Laboratory, Physics Study Programme, Science Department, Sumatra Institute of Technology, Indonesia.

TOPEX Satellite Data Utilization

TOPEX/Poseidon satellite data were retrieved from http://topex.ucsd.edu to generate regional gravity anomaly maps. These anomalies represent deviations from theoretical gravity models and reflect subsurface density contrasts. TOPEX data were selected due to their wide spatial coverage and utility in inaccessible terrains.

Gravity Data Processing Workflow

The gravity data were processed using the following tools and steps:

1. Microsoft Excel: Initial compilation and Bouguer anomaly correction.
2. Oasis Montaj: Terrain correction and spectral analysis.
3. MATLAB: Reduction to a flat plane and anomaly separation.
4. Surfer: Generation of Bouguer anomaly maps, gridding, and visualization of residual and regional anomalies.
5. Grablox: Construction of the 3D gravity inversion model.
6. Bloxer: Editing and interpretation of the 3D model, including fault geometry and density distribution.

Modeling Parameters and Assumptions

The 3D inversion model was constrained by geological boundaries and anomaly segmentation. Density values were categorized as low (1.00–2.55 g/cm^3), moderate (2.22–2.76 g/cm^3), and high (2.72–3.00 g/cm^3). The model assumes isotropic and homogeneous subsurface conditions within each lithological unit. Grid resolution, depth range, and regularization parameters were selected based on prior studies and software defaults, with iterative refinement during inversion.

Limitations

No ground-based gravity measurements were used for calibration. The resolution of TOPEX data may limit the detection of fine-scale structures, and the heat source and basement depth remain unresolved within the current modeling scope.

TOPEX data analysis

TOPEX/Poseidon (Topography Experiment/Poseidon) is a joint satellite mission between NASA and CNES (Centre National d'Études Spatiales, France), launched in 1992 with the primary objective of measuring sea surface topography using radar altimetry. Although originally designed for oceanographic research, data from this mission has been widely applied in geophysical studies, particularly for mapping Earth's gravity field at regional and global scales. In geothermal exploration, TOPEX data is used to generate regional gravity anomalies defined as deviations between observed gravity values and theoretical models (Ismullah et al., 2018; Watlet et al., 2020). These anomalies reflect subsurface rock density variations and assist in identifying geological structures such as faults, basins, and reservoir zones (Iqbal et al., 2023). TOPEX-derived gravity data is especially valuable in areas that are difficult to access via ground-based surveys, enabling preliminary interpretations of regional geological configurations. When integrated with local or residual gravity data, TOPEX contributes significantly to three-dimensional (3D) gravity inversion modeling, enhancing the understanding of geothermal systems and supporting more efficient exploration planning (Watlet et al., 2020).

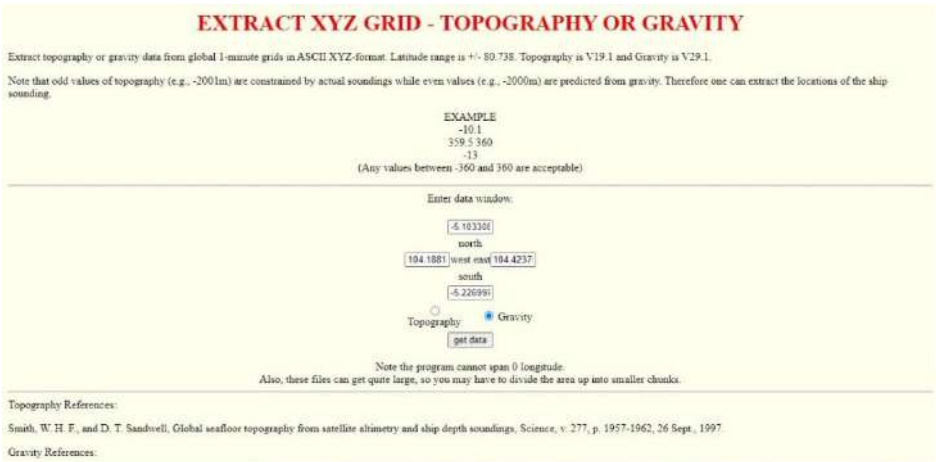

Figure 2. Data collection using TOPEX. The data used in this study is secondary data obtained from TOPEX satellite images. The data was collected from the website http://topex.ucsd.edu/. The data obtained is in the form of topography, gravity and FAA (free air anomaly) data

Secondary data obtained from TOPEX satellite images via the website http://topex.ucsd.edu/ **(Figure 2)** will be processed using several methods. The data processing methods used in this study employ several supporting software programs, such as Microsoft Excel, which is used to combine TOPEX satellite image data and perform simple Bouguer anomaly corrections. Oasis Montaj is used to perform terrain correction calculations and spectrum analysis. Matlab is used in the process of reducing ABL to a flat plane, Surfer is used in the process of creating a complete Bouguer anomaly map before and after reduction to a flat plane, regional anomalies and residual anomalies, creating gridding on the data, Grablox is used in the process of creating a 3D model, Bloxer is used in the process of opening and editing 3D models that will be used together with target anomalies in performing interpretations (Lei et al., 2019; Yu-feng et al., 2021; Zhang et al., 2021).

Data Acquisition

This study was conducted in two main stages: data acquisition and data processing. The data acquisition phase began with a literature review to determine the study area and its geographic coordinates. These coordinates, originally in degrees, minutes, and seconds, were converted into decimal format to ensure compatibility with satellite data systems. The converted coordinates were then entered into the TOPEX (Topography Experiment/Poseidon) satellite data portal to retrieve secondary gravity data in ASCII-XYZ format, which includes longitude, latitude, elevation, and Free-Air Anomaly (FAA) values (Ismullah et al., 2018; Maryanto, 2017; Watlet et al., 2020).

The first stage of data processing was carried out using Microsoft Excel. The TOPEX data were compiled into a spreadsheet, and initial calculations were performed to determine average elevation values and their deviations. A range of rock densities was applied to calculate simple Bouguer anomalies, followed by statistical analysis to evaluate the correlation between gravity anomalies and elevation. This process involved assessing the relationship between density and anomaly variation, which was visualized through a linear graph. From this graph, the Bouguer density used for further corrections was determined .

Subsequently, Bouguer correction was applied to account for the gravitational effect of the mass between the measurement point and the reference datum. The corrected values were used to compute the simple Bouguer anomaly. However, since topographic variations still influenced the results, terrain correction was necessary. This correction was performed using Oasis montaj software, supported by Shuttle Radar Topography Mission (SRTM) data. The SRTM data were first processed in Global Mapper to generate topographic elevation files in a compatible grid format. The terrain correction values were then transferred to Excel for integration with the gravity data.

Once terrain correction was applied, the complete Bouguer anomaly was calculated by combining the corrected FAA values with the terrain data. These results were then converted into Universal Transverse Mercator (UTM) coordinates to facilitate spatial analysis. The complete Bouguer anomaly data were plotted using Surfer software to visualize the distribution of gravity anomalies across the study area.

The final stage involved spectral analysis of the complete Bouguer anomaly data in a flattened spatial domain. This analysis was conducted using Fourier transformation techniques to estimate the depth of regional and residual anomaly sources. The resulting graph displayed the relationship between wave number and amplitude, segmented into regional, residual, and noise components. Each segment was analyzed based on its slope and determination coefficient to interpret the depth and significance of the anomalies.

This methodological approach integrates satellite-derived gravity data with statistical and spectral analysis to construct a comprehensive subsurface model. It enables the identification of fault structures, reservoir zones, and recharge pathways, providing a robust framework for geothermal exploration in the East Sekincau area.

Principles of the Gravity and Analytical Method

The gravitational method is based on Newton's law of gravitation, which states that the gravitational force between two materials with different masses, m_0 and m, separated by a distance $|\vec{r} - \vec{r}_0|$ from the centre of mass is proportional to the product of the different masses and inversely proportional to the square of the distance **(Figure 3)**, which can be written in equation (1).

$$\vec{F}(\vec{r}) = -G\frac{m_0 m(\vec{r}-\vec{r}_0)}{|\vec{r}-\vec{r}_0|^2\,|\vec{r}-\vec{r}_0|} \quad ...(1)$$

$\vec{F}(\vec{r})$ is the force acting on m due to the presence of m_0 in the opposite direction, namely $|\vec{r}-\vec{r}_0|$ where m_0 in *meters*. G is the gravitational constant with a magnitude $6{,}67428 \times 10^{11}\mathrm{Nm^2kg^{-2}}$. Gravitational field is a measurable quantity in gravitational methods. The gravitational field of material m_0 is the magnitude of the force per unit mass at a point at a distance $|\vec{r}-\vec{r}_0|$ from m, which can be written in equation (2).

$$\vec{E}(\vec{r}) = \frac{\vec{F}(\vec{r})}{m(\vec{r})} - G\frac{m_0 m(\vec{r}-\vec{r}_0)}{|\vec{r}-\vec{r}_0|^2\,|\vec{r}-\vec{r}_0|} \quad ...(2)$$

$\vec{E}(\vec{r})$ is the gravitational field, m_0 is the mass of the material, and $|\vec{r}-\vec{r}_0|$ the distance between the point and the centre of mass. The gravitational potential of a collection of masses is the sum of the gravitational forces of each mass (Watlet et al., 2020). The sum of the vectors of the potentials caused by the masses in space is the total force on the material being tested. The gravitational force at the boundary of a continuous mass distribution m can be determined using this principle (Fraser, 1969). A continuous mass distribution m is a collection of very small masses in very large numbers, $dm = (x, y, z)$, which is the density of the mass distribution. The application of the superposition principle can be written in equation (3).

$$U(P) = \gamma \int_v \frac{dm}{r} = \gamma \int_v \frac{\rho(Q)}{r} dv \quad ...(3)$$

The integration covers the volume where the actual volume is located in the mass. U is the gravitational potential, γ is the gravitational constant, P is the observation point, Q is the integration point, r is the distance between P and Q, ρ is density distribution, and the density is in units of g/cm^3. The observation point located outside the mass distribution **(Figure 4)** must be considered. If the density of the mass distribution is good, then the integration in equation (3) is convergent for all P outside the mass, and the differentials x, y, z can be transformed into integral form.

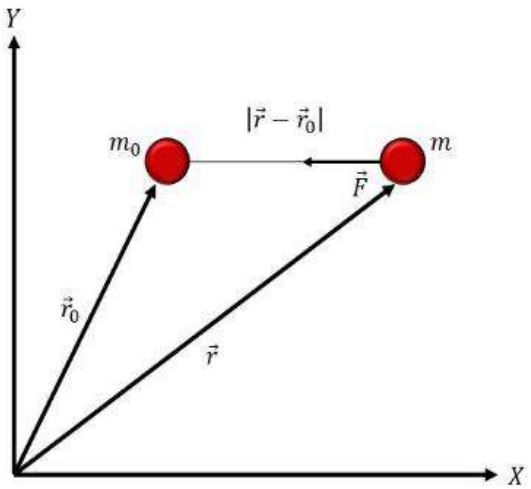

Figure 3. Attractive force between two materials

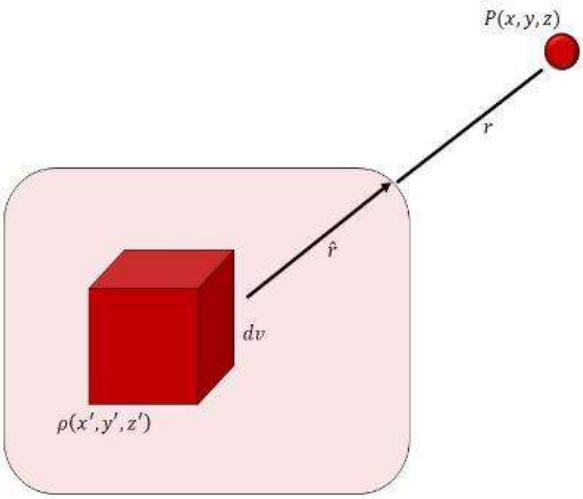

Figure 4. Gravitational force at point P due to density distribution ρ

The bouguer gravity anomaly (BGA) method employs several equations to calculate gravity anomalies by taking into account three stages of correction (C. F. Li, 2011). The first is Free-Air Correction (FAC). This stage is performed to eliminate the topographical or height effects that affect the reading value of the weight force value without considering the effect of the rock mass. The second stage is the Bouguer Correction (BC), which is an elevation correction that takes into account the effect of the mass of rock between the datum surface (geoid) and the survey point. The third stage is Topographic Correction (TC). This correction is made to consider the gravitational field effect of the surrounding topography. During measurement, the topographic elevation around the measurement point, usually within the inner and outer radius, is measured.

RESULTS AND DISCUSSION

Overlay of Topography with Bouguer Anomalies

The Complete Bouguer Anomaly Map (ABL) was obtained through the processing of gravity data in Oasis Montaj. The ABL map depicts the distribution pattern of rock density beneath the earth's surface. The ABL map results for the study area were produced in UTM 46 N coordinates, as shown in **Figure 5**. The colour scale on the ABL map shows the variation in anomaly values in the study area. The ABL map has positive anomaly values with a range of 54.6 mGal to 1015.2 mGal.

The southwestern part of the ABL map shows a high positive anomaly pattern, which indicates that the rocks in this area have a high density. The high anomaly is marked by orange to pink colours with a range of values from 57 anomalies of 310.8 mGal to 1015.2 mGal. Meanwhile, the northeast, east, southeast to northwest parts of Simeulue Island have low positive anomaly values, indicating that this area has a lower density. Low anomalies are marked by blue to yellow colours with anomaly values ranging from 54.6 mGal to 199.1 mGal. The high anomaly pattern in the southwest is a reaction to the pressure arising on the western side of Sumatra Island due to the meeting of the Indo-Australian oceanic plate pushing the Eurasian continental plate at an angle. In addition, high anomalies are identified as rocks that have high density, such as oceanic plates.

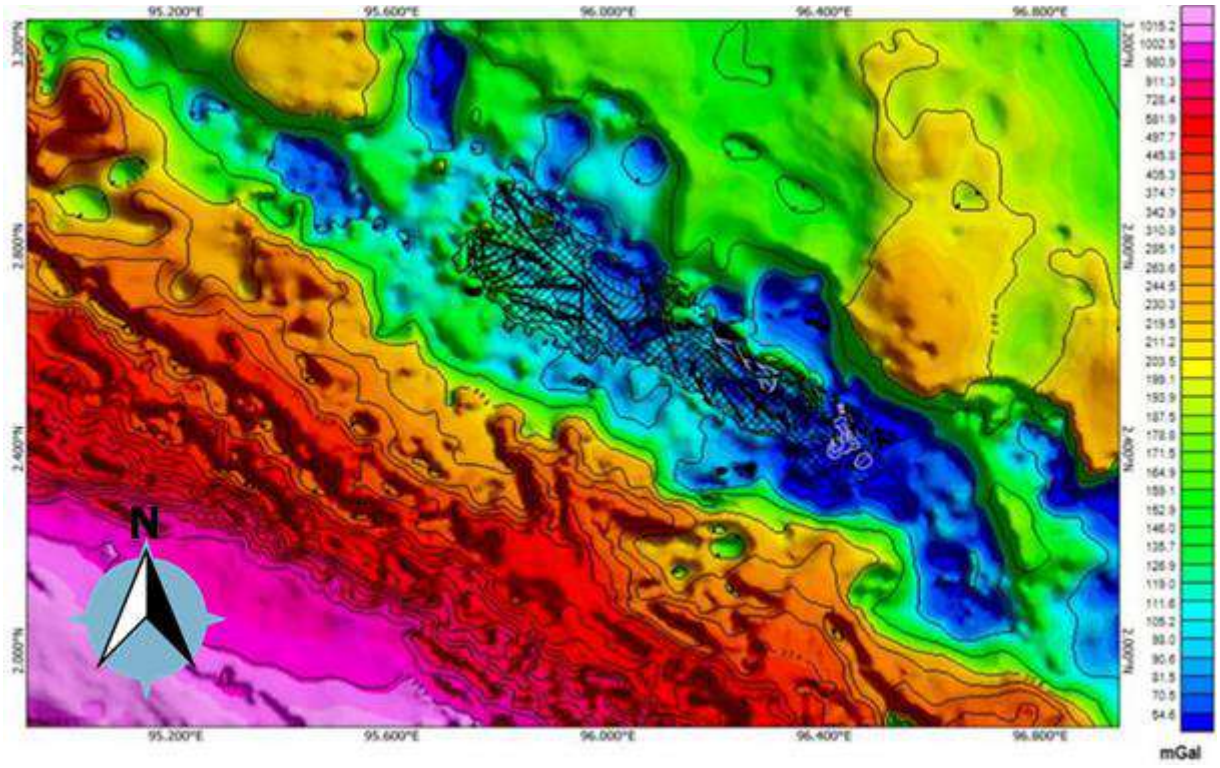

Figure 5. Topographic overlay map with Bouguer gravity anomaly values

High positive anomalies are produced by the relatively shallow position of the Moho in the subduction zone, beneath fragments of continental crust and thin sediments covering the oceanic crust. Oceanic plates have a high density due to their silicon and magnesium content, causing them to subduct beneath continental plates and form subduction zones. In addition to the subduction zone formed by the meeting of the oceanic plate and the continental plate, the meeting of these plates also causes the formation of accretionary prisms, forearc basins, mountain arcs and backarc basins. The accretionary prism area on the complete Bouguer anomaly map is in the form of an anomaly with an orange colour in the southeast to northwest, forming a diagonal direction.

3D Modelling of Gravity Data

In the three-dimensional modelling process, there are two stages, namely forward modelling and inverse modelling. Forward modelling is carried out to create an initial model that describes the area of the study. The area of the study is 247.08 km in the x direction and 153.54 km in the y direction. It is then divided into 20 minor blocks in the x direction and 20 minor blocks in the y

direction, forming 400 minor blocks for each layer. The depth of the block in the vertical z direction is 40.77 km, which is divided into 10 minor blocks. Thus, the total number of minor blocks for all layers is 4000 blocks. The results of forward modelling for the initial model of the study area can be seen in **Figure 6**.

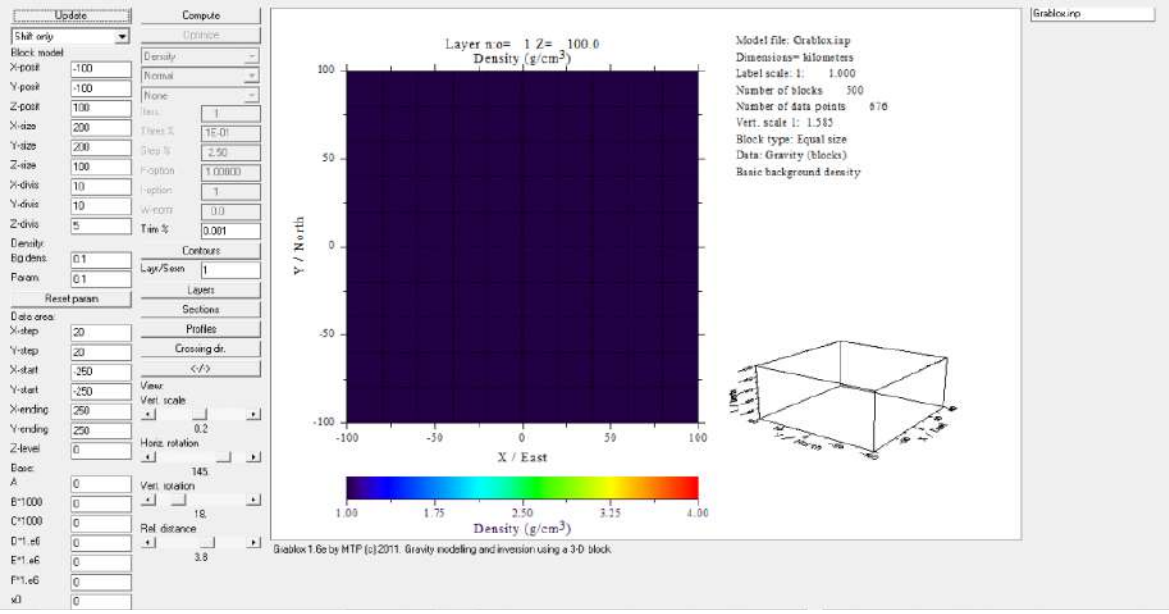

Figure 6. Initial model display in the Grablox 1.6e programme

In the initial model, a rock density range of 1 g/cm^3 to 3.43 g/cm^3 was entered. This density range was entered based on the results of two-dimensional modelling carried out using Oasis Montaj software. The next stage was to perform an inversion process on the initial model. The results of entering the complete Bouguer gravity anomaly measurement data are shown in **Figure 7a**.

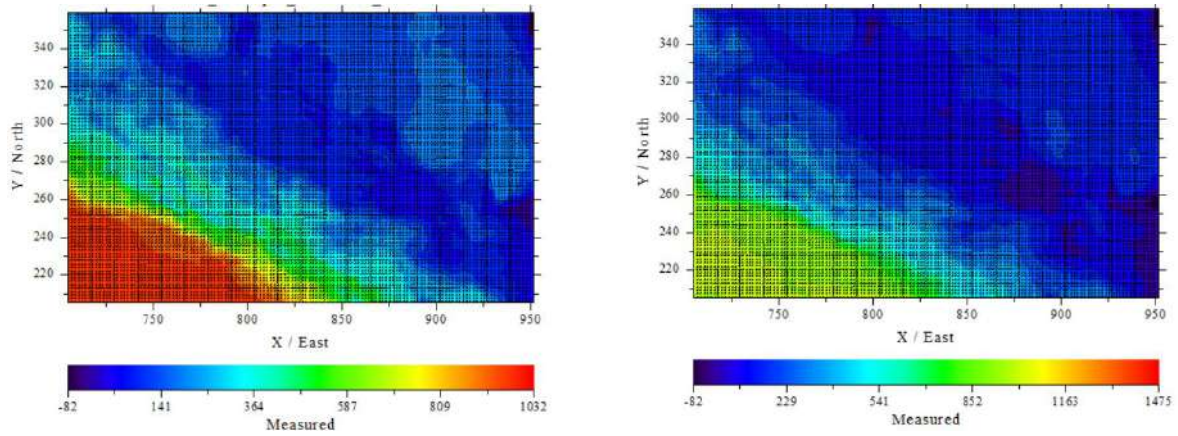

(a) **(b)**

Figure 7. (a). Complete Bouguer anomaly contour map before inversion and **(b)** Results of basic optimisation of complete Bouguer anomaly data

The initial model that had been created previously underwent an optimisation process, starting with base optimisation, density, Occam d (density), height and Occam h (height). The results of the base optimisation shown in **Figure 7b** have an error value of 0.1283%. Base optimisation was carried out to optimise or maximise the basic parameter values in the gravity anomaly. The range of anomaly values in base optimisation is -82 mGal to 1032 mGal. The error value of base optimisation shows that the match between the data at each point has a fairly good accuracy value. This can be stated because the basic parameter values of the gravity anomaly have a small error value.

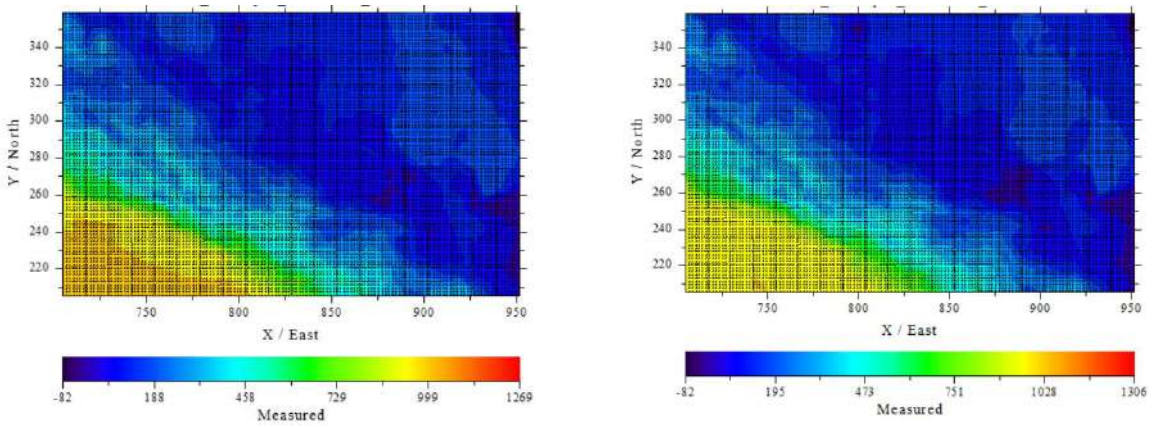

(a) **(b)**

Figure 8. (a). Complete Bouguer anomaly data density optimisation results and **(b)** Results of optimisation of complete Bouguer anomaly data density

Density optimisation was performed to maximise the match between the calculated density values. The results of the density optimisation are shown in **Figure 8a**, with an error value of 0.03223%. The error value of the base optimisation shows that the match between the data at each point has a fairly good accuracy. The range of anomaly values in density optimisation is -82 mGal to 1475 mGal. The contour pattern looks very different in the northwest, north, northeast to southeast. The 3D model to be created requires a model with a smaller error rate, so Occam d (density) optimisation needs to be performed. The results of Occam d (density) optimisation are shown in **Figure 8b**, with an error value of 0.03605%. The range of anomaly values in occam density optimisation is -82 mGal to 1269 mGal. Contour differences are visible in the southeast to northwest of the study area, which is an accretion prism area.

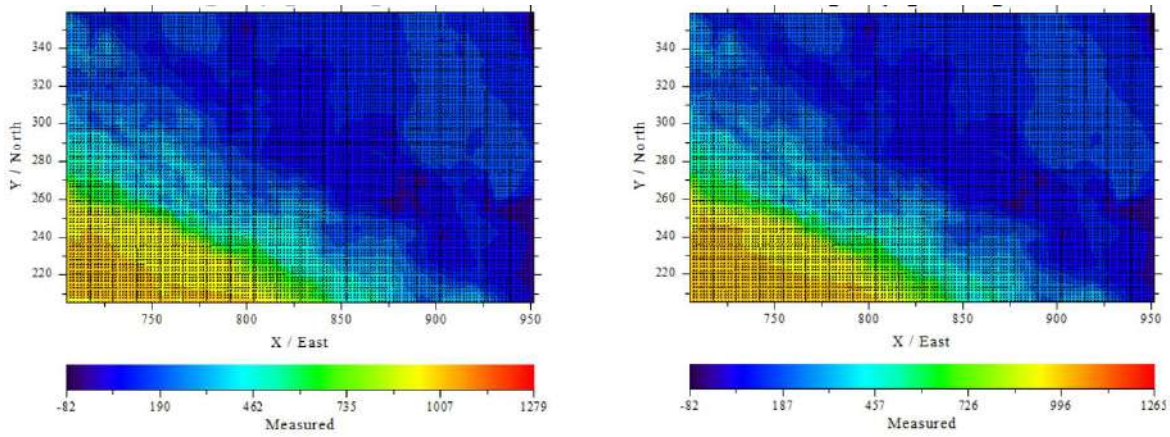

(a) **(b)**

Figure 9. (a). Results of complete Bouguer anomaly data elevation optimisation and **(b)** Results of occam optimisation of complete Bouguer anomaly data

Block height optimisation is performed to maximise the height of minor blocks. The thickness and height of each layer are represented by the height of the block. The results of block height optimisation can be seen in **Figure 9a**, with an error rate of 0.03008%. The range of anomaly values in occam density optimisation has a value range of -82 mGal to 1306 mGal. The difference in contour patterns in the southeast to northwest stretches diagonally, which is included in the accretion prism area. After that, occam height optimisation was carried out with the aim of maximising the height results of each block. The results of occam height optimisation are shown in **Figure 9b** with an error value of 0.03239%. The range of anomaly values in occam density optimisation has a value range of -82 mGal to 1279 mGal. The results of the occam height optimisation show that high anomalies are located in the southwestern part of the study area, while low anomalies are located in the southeastern to northwestern parts of the study area. Occam height optimisation is the final

optimisation of the entire optimisation process in the program used to obtain a Bouguer anomaly pattern that matches the data model. The results of the occam height optimisation will be used for further interpretation as it is a combination of the entire optimisation process (Lei et al., 2019; Yu-feng et al., 2021; Zhang et al., 2021).

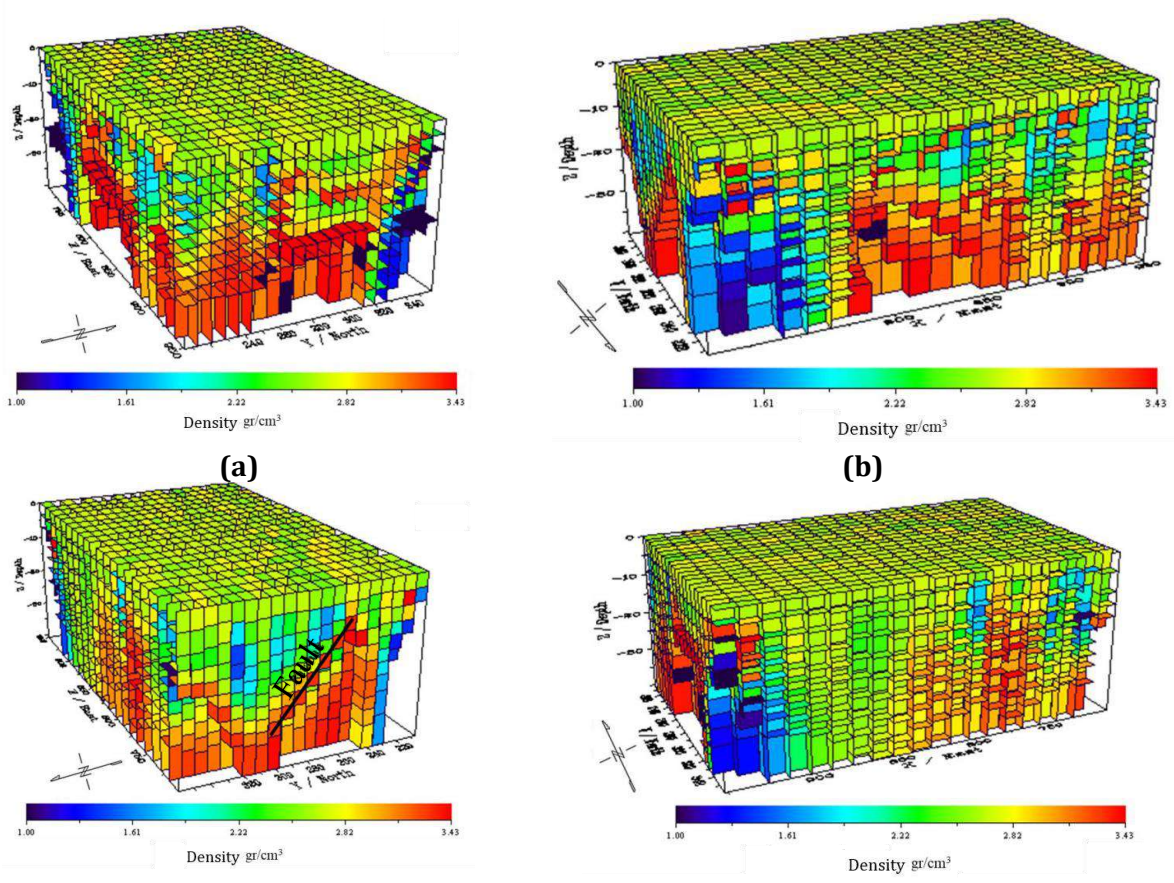

Figure 10. (a). 3D model of the east side;**(b)** North side 3D model; **(c)** West side 3D model and **(d)** South side 3D model

After the forward modelling and inverse modelling processes were completed, the modelling data was entered into Grablox 1.6e software to view the modelling in 3D. The 3D modelling of the subsurface of the island based on complete Bouguer gravity anomalies from several sides can be seen in **Figure 10**. The 3D modelling display resembles ten three-dimensional layers, with a total depth of 40.77 km. The comprehensive 3D model has density variations ranging from 1 g/cm^3 to 3.43 g/cm^3. The density value variations in each block layer are indicated by a colour scale (Lei et al., 2019; Yu-feng et al., 2021; Zhang et al., 2021).

In performing the interpretation, two 3D models in the z-direction were selected to represent the overall shape of the model. The selected 3D models are in the sixth and tenth layers, which can be seen in **Figure 11** and **Figure 12**. The interpretation of the subsurface structure and rock types for 3D modelling was carried out based on geological information and data as well as rock density data.

The fifth layer model shown in **Figure 11** is located at a depth of 16.11 km to 19.92 km. The fifth layer has a density range of 1 g/cm^3 to 3.43 g/cm^3 with an average density of 2.35 g/cm^3. The average density value of the fifth layer can be interpreted as sedimentary rock such as sandstone and shale (Lei et al., 2019; Yu-feng et al., 2021; Zhang et al., 2021). In the fifth layer, high density begins to spread in the southwestern and northwestern parts of the study area. This can be identified as plate subduction in the island area beginning to occur at a depth of 16.11 km. Low density in this layer is located in the central part of the study area, which is the accretion prism area (Iqbal et al., 2023).

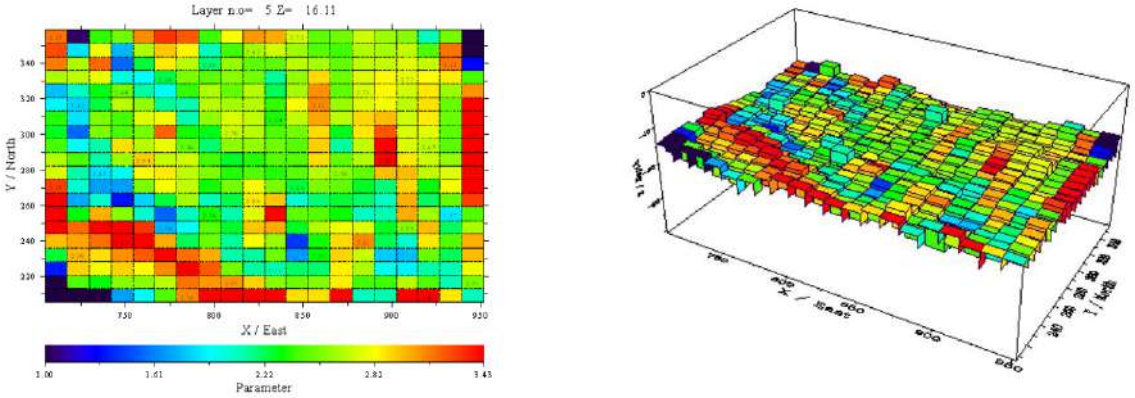

(a) **(b)**

Figure 11. Complete 3D shape of the fifth layer of the Bouguer anomaly **(a).** 2D shape of the fifth layer of the complete Bouguer anomaly based on rock type parameters represented by density. and **(b)** 2D shape that has been adjusted to the topography

The tenth layer model shown in **Figure 12** is located at a depth of 35.26 km to 40.77 km. The tenth layer has a density range of 2.46 g/cm^3 to 3.43 g/cm^3 and an average density of 2.9 g/cm^3. Low density values can be interpreted as sedimentary rocks, while high density values can be interpreted as igneous rocks such as gabbro. The average density value of the tenth layer can be interpreted as igneous rocks consisting of diabase and basalt. For further interpretation, a comparison was made between the subduction form on Simeulue Island, the 2D model, the 3D model on the fifth and tenth layers, and the 3D subduction model of Simeulue Island, which can be seen in **Figure 13**.

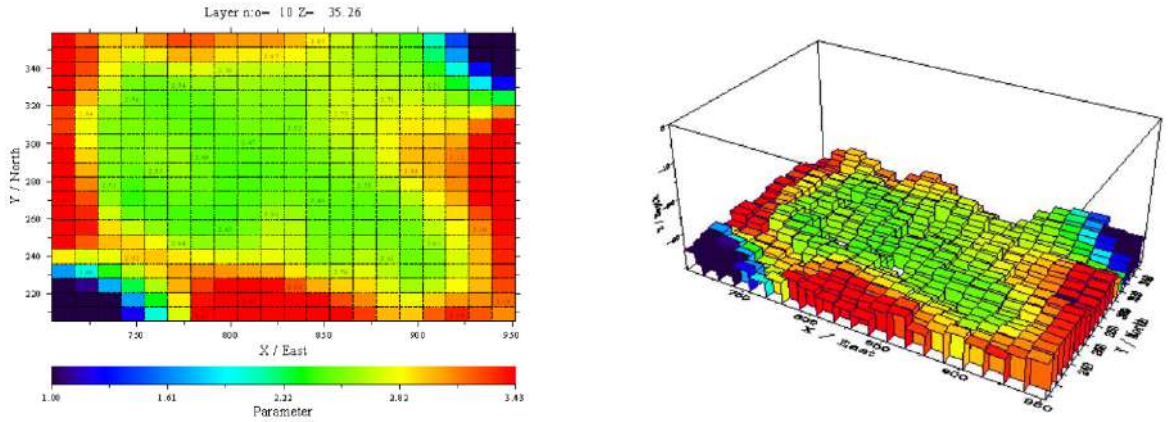

(a) **(b)**

Figure 12. Complete 3D shape of the fifth layer of the Bouguer anomaly **(a).** 2D shape of the fifth layer of the complete Bouguer anomaly based on rock type parameters represented by density. and **(b)** 2D shape that has been adjusted to the topography

The modelling results were further interpreted by comparing the movement patterns of the Simeulue Island subduction plate with the 2D gravity anomaly modelling, as well as the 3D modelling results of the fifth and tenth layers and the overall 3D subduction structure beneath Simeulue Island. This integrated interpretation elucidates the subduction process, including slab geometry, depth variation, and structural characteristics of the subducting plate, providing insights into the tectonic evolution of the region (Kawamoto et al., 2012; C. F. Li, 2011; Obara, 2002), as illustrated in **Figure 13**.

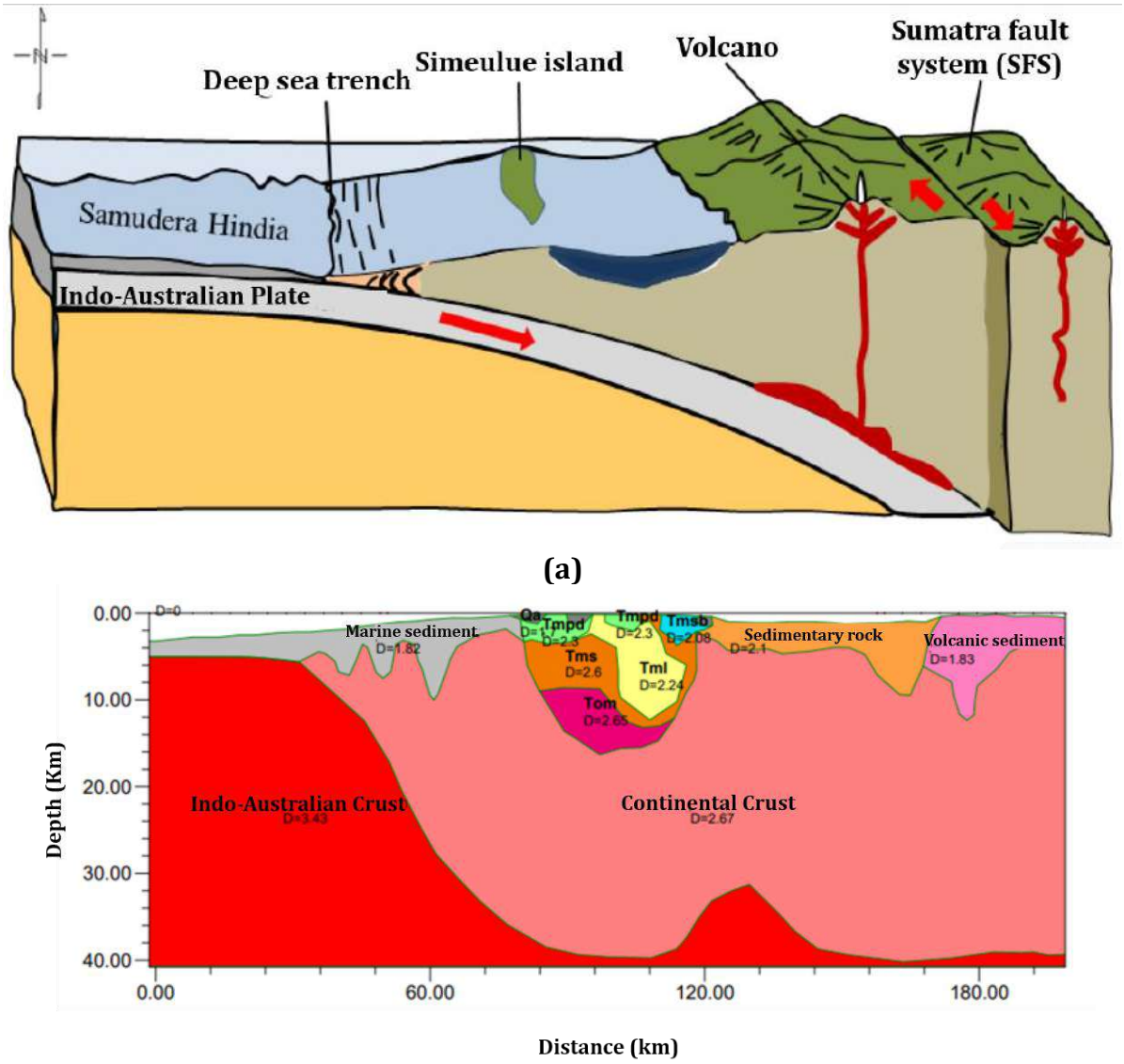

Figure 13. (a) Movement of the Simeulue Island subduction plate, **(b)** 2D modelling of gravity anomalies

CONCLUSION

Based on the research conducted in the Simeulue Island region, several key conclusions can be drawn. The analysis of the complete Bouguer anomaly map reveals high anomaly values in the southwestern part of the study area, attributed to the convergence between the Indo-Australian oceanic plate and the Eurasian continental plate. In contrast, low anomaly values are observed from the southeastern to the northwestern areas, which are part of the accretionary prism zone. The regional anomaly map indicates deep anomaly sources with estimated depths of approximately 11.6 km and anomaly values ranging from 59.8 mGal to 1015.3 mGal. Meanwhile, the residual anomaly map reflects shallow anomaly sources, with estimated depths ranging from 1.63 km to 11.6 km and anomaly values between -52.8 mGal and 51.1 mGal. The low residual anomalies are interpreted to represent sedimentary basins within the study area. Furthermore, the 2D modeling of the complete Bouguer anomaly suggests the presence of subduction, where the oceanic plate with a rock density of 3.43 g/cm^3 descends beneath the continental plate with a density of 2.67 g/cm^3. Beneath Simeulue Island, six geological formations have been identified: Dihit, Layang Baung, Sigulai, Bancuh Kuala Makmur, Aluvium, and Sibigo. The 3D modeling further illustrates the onset of plate subduction at a depth of approximately 16.11 km, with the continental crust thickness in the accretionary prism zone estimated to be around 39 km.

AUTHOR CONTRIBUTIONS

Conceptualization, KCSD and RNS; methodology, TIN; software, ZNP; validation, KCSD, RNS, and TIN; formal analysis, HT; investigation, AI; resources, KCSD; data curation, RNS; writing—original draft preparation, AI; writing—review and editing, ZNP; visualization, HT; supervision, TIN; project administration, RNS; funding acquisition KCSD.

ACKNOWLEDGMENT

The author would like to thank the relevant parties who have provided support for this research.

CONFLICTS OF INTEREST

The authors declare no conflict of interest concerning the publication of this article. The authors also confirm that the data and the article are free of plagiarism.

REFERENCES

Bronto, S., Asmoro, P., Hartono, G., & Sulistiyono, S. (2012). Evolution of Rajabasa Volcano in Kalianda Area and Its Vicinity, South Lampung Regency. *Indonesian Journal on Geoscience*, *7*(1), 11–25. https://doi.org/10.17014/ijog.v7i1.132

Fraser, D. C. (1969). Countouring of VLF-EM data, Geophysics. *Geophysics*, *34*, 958–967.

Gan, F., Han, K., Lan, F., Chen, Y., & Zhang, W. (2017). Multi-geophysical approaches to detect karst channels underground — A case study in Mengzi of Yunnan Province, China. *Journal of Applied Geophysics*, *136*, 91–98. https://doi.org/10.1016/j.jappgeo.2016.10.036

Hariyono, E., & S, L. (2018). The Characteristics of Volcanic Eruption in Indonesia. *Volcanoes - Geological and Geophysical Setting, Theoretical Aspects and Numerical Modeling, Applications to Industry and Their Impact on the Human Health*, *July*. https://doi.org/10.5772/intechopen.71449

He, M. (2014). Latest progress of soft rock mechanics and engineering in China. *Journal of Rock Mechanics and Geotechnical Engineering*, *6*(3), 165–179. https://doi.org/10.1016/j.jrmge.2014.04.005

Iqbal, M., Al-Hassan, M. A., Herdianita, N. R., & Juliarka, B. R. (2023). Determining recharge area in ULUBELU geothermal field, LAMPUNG, Indonesia using stable isotope data. *Applied Geochemistry*, *156*(July), 105763. https://doi.org/10.1016/j.apgeochem.2023.105763

Ismullah, M. F., Massinai, M. A., & Maria. (2018). Shallow Depth Study Using Gravity & Magnetics Data in Central Java - Yogyakarta. *IOP Conf. Series: Journal of Physics: Conf. Series 979*, 012046. https://doi.org/10.1088/1742-6596/979/1/012046

Kawamoto, T., Kanzaki, M., Mibe, K., Matsukage, K. N., & Ono, S. (2012). Separation of supercritical slab-fluids to form aqueous fluid and melt components in subduction zone magmatism. *Proceedings of the National Academy of Sciences of the United States of America*, *109*(46), 18695–18700. https://doi.org/10.1073/pnas.1207687109

Lei, J., Chang-li, Y., Ya-bin, Y., Meng-long, X., Guang-zhi, Z., & Ruo-ye, J. (2019). Optimization algorithm for rapid 3D gravity inversion*. *Applied Geophysics*, *16*(4), 507–518. https://doi.org/10.1007/s11770-019-0781-2

Li, C. F. (2011). An integrated geodynamic model of the Nankai subduction zone and neighboring regions from geophysical inversion and modeling. *Journal of Geodynamics*, *51*(1), 64–80. https://doi.org/10.1016/j.jog.2010.08.003

Li, H., Zhai, M., Zhang, L., Gao, L., Yang, Z., Zhou, Y., He, J., Liang, J., Zhou, L., & Voudouris, P. C. (2014). Distribution, microfabric, and geochemical characteristics of siliceous rocks in central orogenic belt, China: Implications for a hydrothermal sedimentation model. *Scientific World Journal*,

2014. https://doi.org/10.1155/2014/780910

Maryanto, S. (2017). Geo Techno Park potential at Arjuno-Welirang Volcano hosted geothermal area, Batu, East Java, Indonesia (Multi geophysical approach). *AIP Conference Proceedings*, *1908*(2017). https://doi.org/10.1063/1.5012712

Nishimura, S., Nishida, J., Yokoyama, T., & Hehuwat, F. (1986). Neo-tectonics of the Strait of Sunda, Indonesia. *Journal of Southeast Asian Earth Sciences*, *1*(2), 81–91. https://doi.org/10.1016/0743-9547(86)90023-1

Obara, K. (2002). Nonvolcanic deep tremor associated with subduction in southwest Japan. *Science*, *296*(5573), 1679–1681. https://doi.org/10.1126/science.1070378

Rizki, R., Ashuri, W., Hakim, R. A., & Santoso, N. A. (2022). Subsurface Survey of Cisarua Lampung Hot Springs Using Geochemical and Gradio-Magnetic Method. *JGE (Jurnal Geofisika Eksplorasi)*, *8*(1), 58–66. https://doi.org/10.23960/jge.v8i1.176

Siregar, R. N., Widana, K. S., & Sismanto. (2022). Radiogenic heat production of S-type and I-type granite rocks in Bangka Island, Indonesia. *Kuwait Journal of Science*, *49*(3), 1–11. https://doi.org/10.48129/kjs.15423

Stern, R. J. (2018). The evolution of plate tectonics. *Philosophical Transactions of the Royal Society A: Mathematical, Physical and Engineering Sciences*, *376*(2132). https://doi.org/10.1098/rsta.2017.0406

Tabei, T., Hashimoto, M., Miyazaki, S., Hirahara, K., Kimata, F., Matsushima, T., Tanaka, T., Eguchi, Y., Takaya, T., Hoso, Y., Ohya, F., & Kato, T. (2002). Subsurface structure and faulting of the Median Tectonic Line, southwest Japan inferred from GPS velocity field. *Earth, Planets and Space*, *54*(11), 1065–1070. https://doi.org/10.1186/BF03353303

Taira, A. (2001). Tectonic evolution of the Japanese island arc system. *Annual Review of Earth and Planetary Sciences*, *29*, 109–134. https://doi.org/10.1146/annurev.earth.29.1.109

Triani, Umam, R., & Sismanto. (2021). 3D Modeling of Subsurface Lawanopo Fault in Southeast Sulawesi, Indonesia Using Grablox and its Consequence to Geohazard. *Indonesian Journal of Geography*, *53*(1), 67–77. https://doi.org/10.22146/IJG.50878

Utama, H. W., Mulyasari, R., & Said, Y. M. (2021). Geothermal Potential on Sumatra Fault System To Sustainable Geotourism in West Sumatra. *JGE (Jurnal Geofisika Eksplorasi)*, *7*(2), 126–137. https://doi.org/10.23960/jge.v7i2.128

Watlet, A., Van Camp, M., Francis, O., Poulain, A., Rochez, G., Hallet, V., Quinif, Y., & Kaufmann, O. (2020). Gravity Monitoring of Underground Flash Flood Events to Study Their Impact on Groundwater Recharge and the Distribution of Karst Voids. *Water Resources Research*, *56*(4), 1–18. https://doi.org/10.1029/2019WR026673

Yan, Y., Zhang, Z., Zhou, X., Wang, G., He, M., Tian, J., Dong, J., Li, J., Bai, Y., Zeng, Z., Wang, Y., Yao, B., Xing, G., Cui, S., & Shi, Z. (2024). Geochemical characteristics of hot springs in active fault zones within the northern Sichuan-Yunnan block: Geochemical evidence for tectonic activity. *Journal of Hydrology*, *635*(December 2023), 131179. https://doi.org/10.1016/j.jhydrol.2024.131179

Yu-feng, W., Yu-jie, Z., Li-hua, F., & Hong-wei, L. (2021). Three-dimensional gravity inversion based on 3D U-Net ++*. *Applied Geophysics*, *18*(4), 451–460. https://doi.org/10.1007/s11770-021-0909-z

Zhang, Z., Yao, H., Wang, W., & Liu, C. (2021). 3-D Crustal Azimuthal Anisotropy Reveals Multi-Stage Deformation Processes of the Sichuan Basin and Its Adjacent Journal of Geophysical Research : Solid Earth. *Journal of Geophysical Research: Solid Earth*, *127*(e2021JB023289), 1–17. https://doi.org/10.1029/2021JB023289

Zheng, H., Luo, J., Zhang, Y., Feng, J., Zeng, Y., & Wang, M. (2021). Geological Characteristics and Distribution of Granite Geothermal Reservoir in Southeast Coastal Areas in China. *Frontiers in Earth Science*, *9*(August), 1–18. https://doi.org/10.3389/feart.2021.683696